

Q1 1 **A 3D-Printed Computer**Q2 2 *Vahideh Shirmohammadli and Behraad Bahreyni**

Vast amounts of data are generated by sensors that are used to monitor people, animals, plants, machines, structures, and the environment. Increasingly, this data is used to create relevant context based on sophisticated pattern recognition algorithms trained using past labeled data. However, most of these sensor systems are severely constrained regarding their communication and computation capabilities due to limitations on available energy, size, or location. New computational approaches are needed to overcome the limitations of existing digital processors in contextual processing. This article discusses the development of the first such computer that is entirely made based on common 3D-printing materials and techniques. It is demonstrated that a simple structure printed with regular 3D printers can be driven and used with common measurement tools to perform sophisticated contextual computations, including standard benchmarks and a demonstration of user activity detection from sensor data. The correlation between memory capacity, nonlinearity, and sampling rates with this computer is examined. The 3D-printed structure may be used as a stand-alone computer to detect patterns in general data streams. Moreover, the computer can be integrated with the sensorized 3D-printed structures, leading to the development of cognizant 3D-printed systems comprising sensors and contextual processors.

research for unconventional computing methods such as neuromorphic or quantum computing.^[2,3] Two rapidly growing areas that rely on unconventional computation methods are in-sensor and near-sensor computing.^[4] Various forms of wireless sensor networks, such as wearables and Internet-of-Things (IoT) modules, use sensors to monitor their surroundings. The data produced by these sensors are often used to create contextual information such as user activity or machine health monitoring. In contrast to brain simulators, cognition in sensing applications is about distinguishing between a limited number of situations of interest. Complex machine learning algorithms used in these applications need to process the mostly redundant data, either locally or remotely, adding a significant power burden during the processing and communicating the sensor data. The recent efforts to develop neuromorphic or in/near-sensor computing methods aim to utilize the physics and structure of the materials and devices to limit the reliance on general-purpose processors. Besides


the savings on energy usage, this approach enables a real-time, context-based response from the sensor module when needed without reliance on communication networks or remote computers.

Reservoir computing (RC) is a computational framework that is well suited to physical implementations of contextual computers.^[5,6] The computational core of a reservoir computer is made of nonlinear neurons with both feedback and feedforward connections, resembling a recurrent neural network (RNN). The connections between the (physical) neurons occur through some sort of information (i.e., energy) exchange between them. The feedback connections in RNN and RC provide a notion of time and memory, making them suitable for processing time-series data. Contrasting an RNN, the weights of the couplings between the neurons in an RC are fixed, and the training is conducted only on the weights of the output layer. This makes the training of RC much simpler and more robust than RNNs, typically requiring simple algorithms such as linear regression. Unlike the traditional von Neumann architectures, the merging of memory with computation units means reservoir computers do not need separate memory to store or communicate data.^[4] In physical realizations of RCs, the material or device physics are employed to nonlinearly map input data onto a high-dimensional space where different events may be distinguished from each other. Physical RC systems have been developed based on mechanical oscillators,^[7–9] memristors,^[10–12] photonic

22 **1. Introduction**

23 The von Neumann architecture, where a computer is constructed
24 from separate units for memory, arithmetic, and program control
25 to perform computations sequentially, has been the engine
26 behind the digital transformation.^[1] Within this architecture,
27 computation capability is increased through running the circuits
28 at higher speeds or by adding computation cores and on-chip
29 memory. The approaching physical limits in semiconductor
30 manufacturing, the inherent requirement for sequential processing,
31 and suboptimal performance while implementing certain
32 algorithms, among other deficiencies, have motivated the

V. Shirmohammadli, B. Bahreyni
Faculty of Applied Sciences
Simon Fraser University
MSE 4176, 250-13450 102nd Ave, Surrey, BC V3T 0A3, Canada
E-mail: bba19@sfu.ca

 The ORCID identification number(s) for the author(s) of this article can be found under <https://doi.org/10.1002/aisy.202300015>.

© 2023 The Authors. Advanced Intelligent Systems published by Wiley-VCH GmbH. This is an open access article under the terms of the Creative Commons Attribution License, which permits use, distribution and reproduction in any medium, provided the original work is properly cited.

DOI: 10.1002/aisy.202300015

1 circuits,^[13,14] carbon nanotube/polymer composites,^[15,16] and
2 connected atomic switches.^[17] These implementations, however,
3 rely on sophisticated interfaces and remain unsuitable for
4 widescale deployment.

5 3D printing enables rapid fabrication of complex, multilayer,
6 and even multimaterial structures at once using various printable
7 materials.^[18] Advances in 3D printing technologies and additive
8 manufacturing have been utilized to develop 3D-printed sensors
9 and hence, 3D-printed smart systems (i.e., structures with
10 embedded sensing capabilities).^[19] However, typical 3D-printed
11 systems, including 3D-printed sensors, are generally passive
12 components, void of computational capability. The desire to
13 add computation capability in analog or digital domains has
14 motivated the research on developing 3D-printed transistors
15 and active components.^[20] Much of this research has thus far
16 focused on developing transistors for analog signal processing
17 or conventional von Neuman digital processors. However, these
18 transistors are printed at much lower densities than the existing
19 silicon microelectronic chips, severely limiting their utility as
20 computational elements. Alternatively, 3D-printed neuromor-
21 phic devices and processors have been proposed as potential
22 methods to add computing power to 3D-printed structures.^[21–23]
23 3D-printed optical signal processors have been proposed to cir-
24 cumvent the challenges on the electrical side for processing large
25 quantities of input data.^[24] Nonetheless, the existing solutions
26 for signal processing with 3D-printed structures either face
27 significant challenges in scaling up the computation capabilities
28 or require sophisticated tools to recover the processed data.

29 In this article, we describe the design and operating principles
30 of a contextual computer that is made through standard 3D print-
31 ing with simple electrical ports for the input and output stages.
32 Despite its simplicity, the computer can tackle complex standard
33 tests and is used to solve the practical problem of user activity
34 detection. Adding to the computational capability of the demon-
35 strated computer is simply achievable by printing additional
36 computational nodes. At a material cost of less than \$1, this com-
37 puter can be used next to existing smart systems for contextual
38 signal processing. It can also be embedded within the structure
39 of 3D-printed intelligent systems, enabling the realization of
40 cognizant 3D-printed systems.

41 2. Results

42 Echo State Networks (ESN) form a particular group of RCs with
43 requirements that can be met using physical components.
44 Within an ESN, the reservoir should be built from coupled non-
45 linear nodes with fading memory.^[5,25] The dynamic response of
46 physical systems often satisfies the fading memory requirement
47 for ESNs when the data are applied or collected at a sampling rate
48 proportional to the response time of the system. The coupling
49 requirement can be met by letting energy transfer from one
50 device to the others nearby. Therefore, it is possible to build phys-
51 ical RCs that utilize various forms of nonlinearity and coupling.

52 The nonlinearity in the current–voltage response of regular
53 thermistors (i.e., temperature-sensitive resistors) due to self-
54 heating is a well-known phenomenon. Within the scope of
55 RC, thermistors can be viewed as a particular form of memris-
56 tors, where the thermal response of the material affects its

electrical behavior. Researchers recently demonstrated an RC 1
that was built using off-the-shelf thermistors that provided the 2
nonlinear response and fading memory requirements while 3
the coupling between the elements was achieved by directional 4
sharing of the electrical current.^[26,27] 5

3D-printed resistors exhibit interesting time-dependent, non- 6
linear responses. These resistors can be made, for instance, from 7
a conductive material using fused deposition modeling (FDM) 8
technology. FDM is presently the most common 3D printing 9
technology, where a filament of the printed material is melted 10
and deposited selectively using a printer head. The nozzle tem- 11
perature for printing these conductive filaments is between 120 12
and 250 °C, depending on type.^[28] However, printed resistors 13
exhibit significant nonlinear responses due to self-heating at 14
much lower temperatures (50–60 °C). **Figure 1** shows the 15
response of a 3D-printed resistor under different conditions. 16
As can be seen, these resistors exhibit a nonlinear response 17
under high currents due to self-heating. Additionally, the 18
resistors exhibit a time-dependent response if the time spent 19
at each current level is shorter than the time needed for reaching 20
thermal equilibrium. The nonlinearity and time dependence in 21
resistors' responses make 3D-printed resistors suitable candi- 22
dates for developing RC computers based on ESN topology. 23
The additional requirement for coupling between the nodes 24
can be achieved in electrical or thermal domains. To achieve this, 25
we printed several resistors close to each other such that the heat 26
generated by one would reach and affect its nearby devices. The 27
reservoir structure can be interpreted as a three-layer neural net- 28
work, in which the weighted connections between the neurons 29
are realized through thermal coupling. Moreover, the nodes on 30
each layer are electrically coupled to each other. Three layers of 31
conductive traces printed of carbon–polylactic acid (PLA) com- 32
posite were stacked on top of each other with a gap in between, 33
filled with pure PLA as the insulating material, as shown in 34
Figure 2. The nonlinear, time-dependent responses of these 35
resistors and the coupling between them satisfy the require- 36
ments for building an ESN. Large contact pads were used to apply 37
the input signals or to read the data from specific nodes. The 38
input layer is driven by an analogue shift register which shifts 39
the input signal multiple times and maps the generated signals 40
to the reservoir. The output layer is trained by running a linear 41
regression on all the outputs from the reservoir. 42

Three samples with similar lateral dimensions that differed 43
only in the thickness of the conductive layers were 3D printed. 44
The thicknesses of the conductive traces in samples 1–3 were 2, 45
1, and 0.5 mm, respectively. These structures were initially stud- 46
ied to evaluate the nonlinearities and time dependences of the 47
responses of neurons at different locations and the couplings 48
between them. **Figure 3** shows test results from these samples 49
on individual neurons' responses to electrical excitations. It 50
was observed that the responses of the neurons might be affected 51
by injecting a control current, I_C , into different nodes in the 52
structure (**Figure 3c**). This effect may be used to bias different 53
neurons postfabrication to make them respond differently from 54
other similarly fabricated devices, adding another parameter that 55
can be used to enhance the reservoir complexity. 56

Figure 3e demonstrates the measured electrical and thermal 57
responses of a resistor on the top layer of the 3D-printed proces- 58
sor over time due to a step current input. After the injection of 59

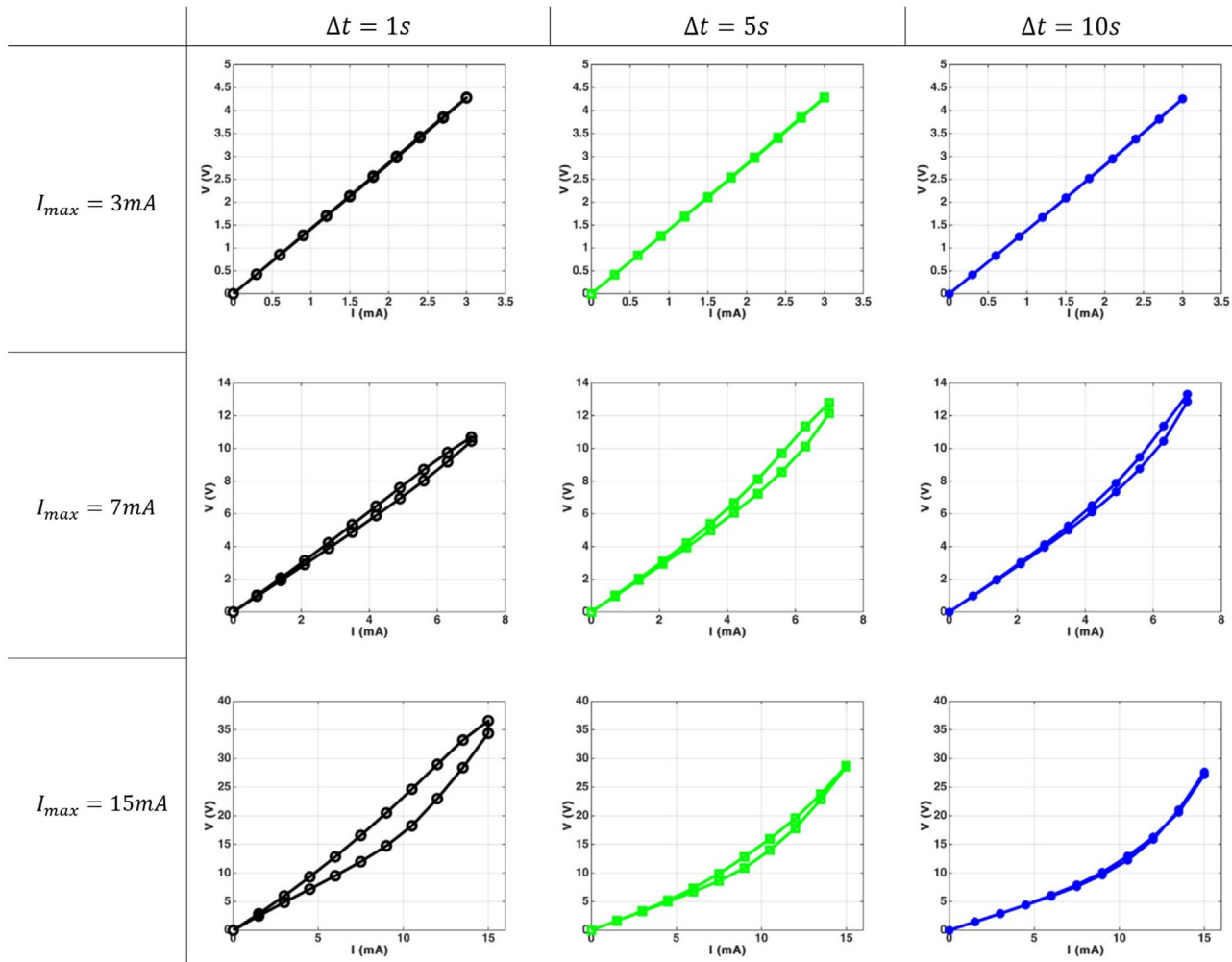


Figure 1. The current–voltage characteristic response of a free-hold 3D-printed resistor under different test conditions. In each case, the current through the resistor was increased in steps from zero up to the maximum value I_{max} (indicated on the left) and back to zero. The current through the resistors was held constant for a period of Δt (indicated at the top) before measuring the voltage across the resistor and proceeding to the next step. It is noteworthy that under these test conditions, the resistor response is repeatable, indicating a permanent change to material response has not yet occurred.

1 the current, both the voltage across the resistor and its tempera-
 2 ture slowly rise until thermal equilibrium with the environment
 3 is reached. In this case, the resistor exhibited a thermal time
 4 constant (TTC) of ≈ 62 s. The TTC will be different for different
 5 neurons in the structure and will depend on the thermal bound-
 6 ary conditions, such as being embedded within the structure or
 7 being exposed to the environment on one or more surfaces. This
 8 property, too, adds a degree of randomness and helps with using
 9 the 3D-printed structure as a contextual processor.

10 Reservoir richness (i.e., the combination of the number of
 11 neurons, their interconnections, and their memory capacity
 12 [MC]) determines its ability to tackle complex computations.
 13 The neurons in the printed reservoir exhibited both linear and
 14 nonlinear responses to different ranges of input signals, as
 15 expected. **Figure 4** demonstrates some characterization results
 16 for sample 3. A single printed computer provides numerous
 17 possibilities to arrange input and output layers by applying or
 18 reading signals to different contacts (Figure 4a–c). Figure 4d

illustrates thermal images of the reservoir at different instances 1
 of time after the application of an input to the reservoir, showing 2
 the evolution of reservoir characteristics through heating and its 3
 subsequent effect on the I – V characteristics of the neurons. 4
 Figure 4e shows samples of an incoming time-series signal, 5
 its time-shifted copies applied to the reservoir, and finally, the 6
 reservoir outputs. During normal operation, the RC distin- 7
 guishes between different events after combining the reservoir 8
 outputs using weights calculated during the training stage. 9
 Video S1, Supporting Information, shows a thermal video of 10
 the computer during its operation in real time. Video S2, 11
 Supporting Information, includes the real-time measurements 12
 of the signals from the computer as it performs computations. 13

2.1. Performance Evaluation Based on Standard Benchmarks 14

The computational capability of the proposed processor to solve a 15
 nonlinear problem which requires a memory of past events can 16

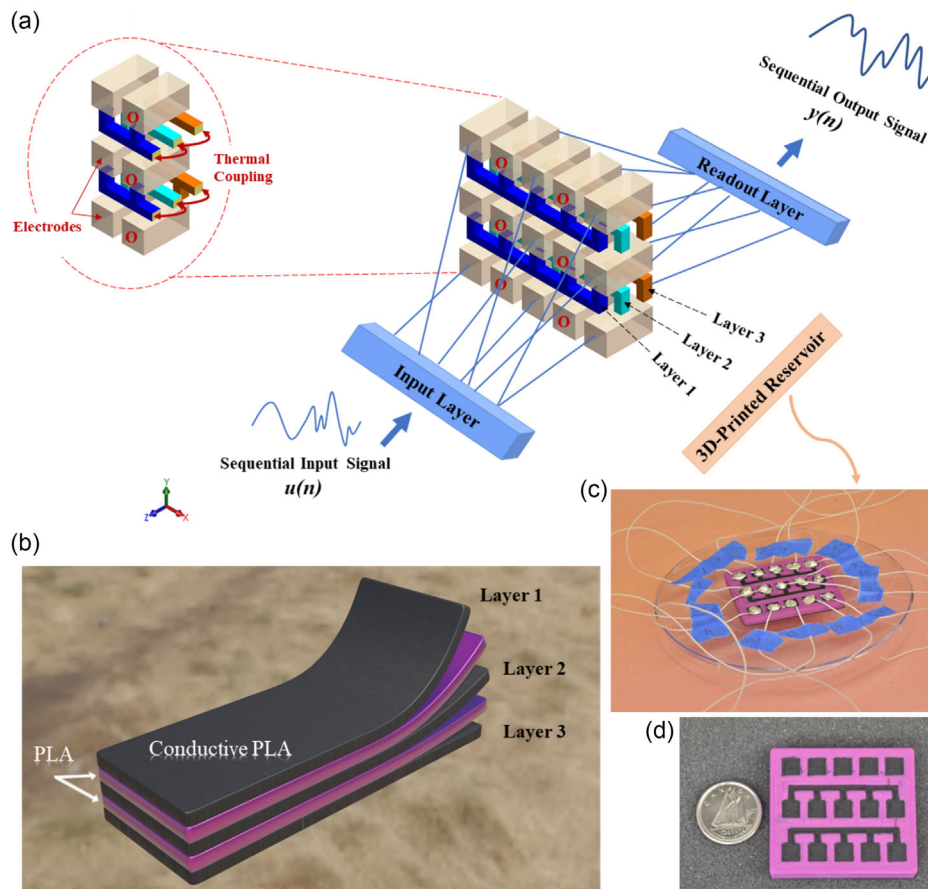


Figure 2. Components of the 3D-printed computer. a) The proposed reservoir structure; b) the layer view of the 3D-printed reservoir in which the heated conductive layers (black) allows for a thermal flow to the coupled layers through PLA (pink); c) the 3D-printed reservoir with electrical connections for applying or reading electrical signals; d) top view of the computer with three conductive layers printed between the insulating material next to a Canadian C10 coin.

1 be evaluated using a nonlinear autoregressive moving average
2 (NARMA) task.^[29,30] The goal of a NARMA task of order n
3 (i.e., NARMA n) is to predict the next point in a time-series signal
4 that is produced using a nonlinear combination of the past
5 events, where n indicates both the order of the nonlinearity
6 and the amount of memory required by the problem
7 (see Experimental Section). The generated dataset includes
8 360 samples. Two hundred fifty samples from this data
9 ($\approx 70\%$) were randomly selected and used to train the output
10 layer weights. The remainder of the dataset was used to validate
11 the computer performance. **Figure 5a** shows the response and
12 the analysis of the response of the 3D-printed processor to
13 NARMA tasks of varying order ($n = 1 \dots 10$). This simple proces-
14 sor with only 18 nonlinear neurons demonstrates good perfor-
15 mance for $n \leq 7$. The performance of the processor can be
16 improved through several simple approaches, including adding
17 additional computational nodes, adding complexity through vary-
18 ing the control signal, or time-multiplexing the tasks between
19 parallel computers.

20 The NARMA test also helps study the compromise between
21 the input signal's sampling rate and retainable memory with
22 the system.^[31] The system state approaches thermal equilibrium

at a slow sampling rate (i.e., low data rate). Although the reservoir 1
exhibits the most nonlinear response in this case, and hence the 2
ability to solve complex problems, it may have lost information 3
about distant past events. On the other hand, a fast sampling rate 4
(i.e., high data rate) reduces the reservoir nonlinearity needed for 5
contextual computing but helps the system retain more informa- 6
tion about past events. Figure 5b,c demonstrates the perfor- 7
mance of the reservoir in solving NARMA tasks of varying 8
orders with different sampling rates. As can be seen, both fast 9
and slow sampling rates result in larger errors. Therefore, proper 10
selection of sampling frequency is essential in achieving optimal 11
performance from the reservoir in terms of its accuracy. 12

The performance of a contextual computer while processing 13
temporal data can be quantified through a concept known as 14
MC, defined as the ability of a processor to retrieve past informa- 15
tion from the reservoir using the linear combinations of its inter- 16
nal states. Figure 5d demonstrates how the MC of the reservoir is 17
affected by the sampling frequency when solving a NARMA3 18
task. As can be seen, a slow sampling rate results in the computer 19
operating with the least error (because of the increased nonline- 20
arity) but also a small MC (≈ 2) because the system forgets about 21
past events. On the other hand, a high sampling rate results in 22

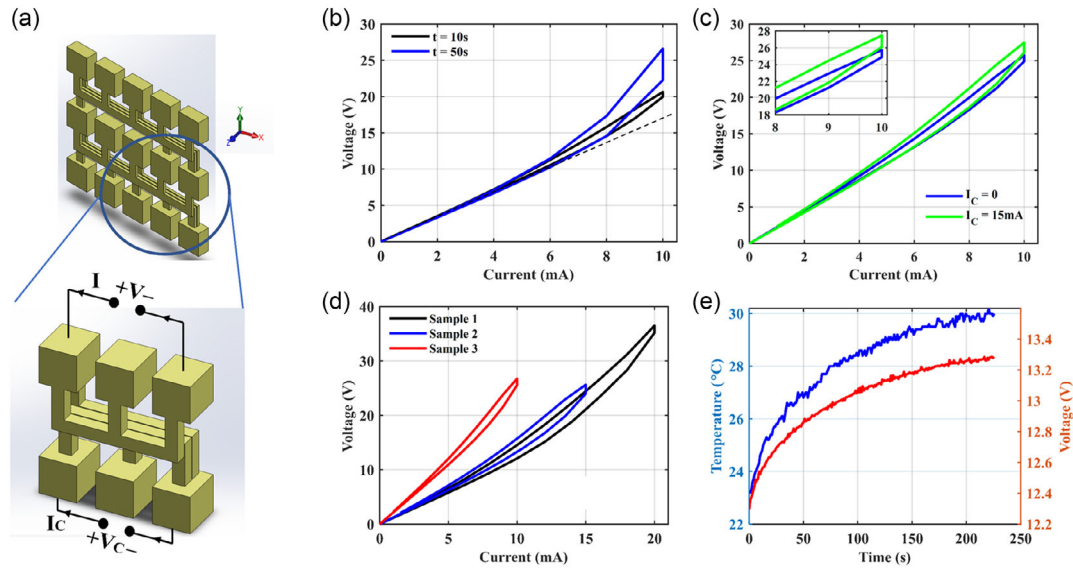


Figure 3. Electrical response of printed structures. a) Schematic of the conductive paths in the fabricated reservoir and its close-up view; b) the nonlinear I - V response of the reservoir obtained by sweeping a current through two of the resistors in steps with a time delay of 10 or 50s between the steps; c) the effect of control current, I_C , on the response of a resistor; d) comparison of the I - V responses of three reservoir samples with similar lateral dimensions but different thicknesses for the conductive traces e) Temperature and the voltage across the two electrodes over time in response to an $I = 8$ mA step current input.

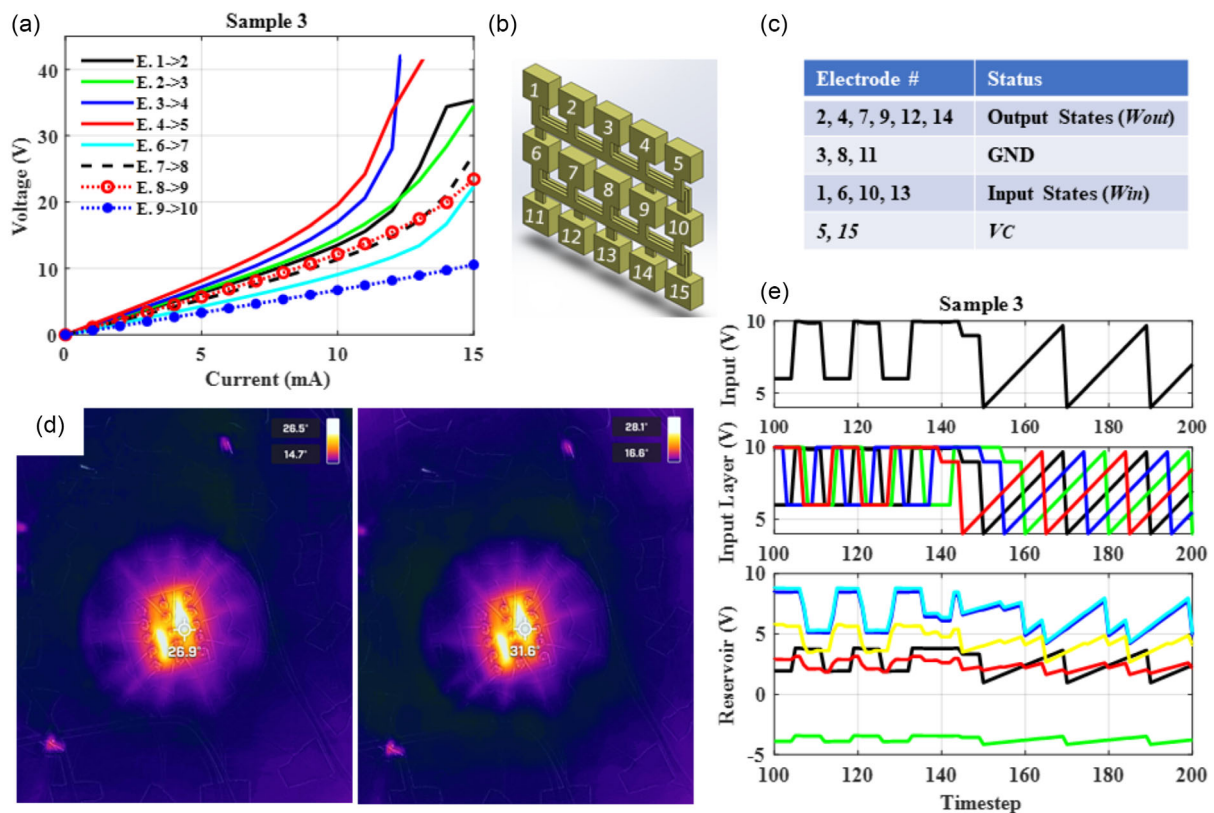


Figure 4. Electrical and thermal response of coupled components. a) I - V characteristics of various pairs of electrodes; b) the electrode labels; c) arrangement of the electrodes in the reservoir and their functions; d) thermal image of the reservoir at different computation times; and e) a sample time-series signal (top), its time-shifted copies applied to the reservoir input by the analogue shift register (middle), and the reservoir output (bottom).

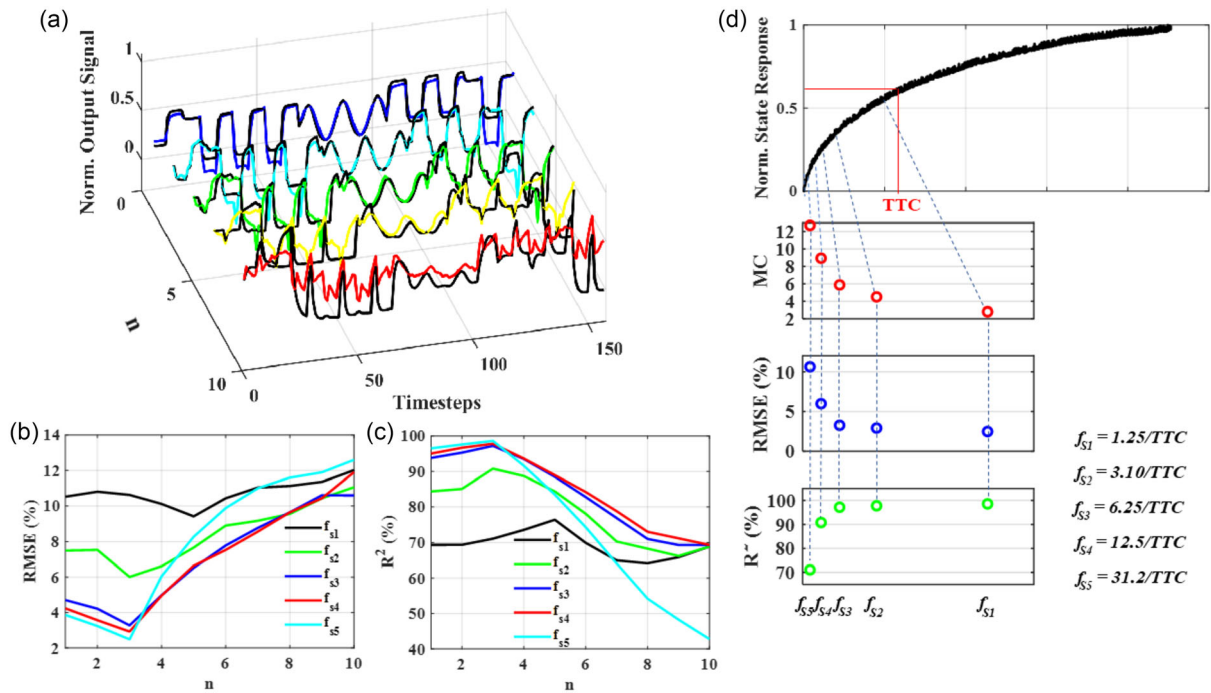


Figure 5. Assessment of the computer performance to solve computational tasks with varying orders of nonlinearity and memory. a) The reservoir response to predicting a time-series input produced by varying orders of NARMA task with $f_s = f_{s3}$. b,c) Comparison of the reservoir performance when solving NARMA tasks of different orders with different sampling frequencies. d) Demonstration of the dependence of reservoir memory capacity, RMSE, and R^2 to sampling frequency when solving a NARMA5 task. The graph at the top shows a typical step response of one of the nonlinear neurons in the reservoir which is used to estimate TTC and set sampling frequencies.

1 poor accuracy, but the system remembers many past events
2 (≈ 12). For this reservoir, a balance may be struck by choosing
3 a sampling frequency around $6/TTC$ to achieve good computa-
4 tion accuracy with a high MC (≈ 6).

5 In general, the optimal performance of physical computers
6 depends on the combination of network complexity, sampling
7 rate, and nonlinearity. The computers need to be designed to
8 attain a certain level of performance through their physical
9 design and optimizing dimensions, number of neurons, types
10 of materials, and other parameters that affect their nonlinearity
11 and time responses.

12 To demonstrate the need for memory integrated within the
13 reservoir, we compared the performance of the 3D-printed
14 processor with two representative regular feedforward neural
15 network (FNN) constructed in MATLAB, which lacks the ability
16 to store and retain temporal information. The results (Figure 6)
17 demonstrate that the 3D-printed processor outperformed the
18 FNN, which consisted of three hidden layers on neurons with
19 a sigmoid activation function. Two FNNs with 18 and 50 neurons
20 were built, trained, and compared with the 3D-printed computer.
21 Increasing the number of neurons in the FNN marginally
22 improves its performance, but it cannot match that of the 3D-
23 printed processor. Even though further optimization of the
24 FNNs with regard to their number of neurons, activation func-
25 tions, and number of layers is likely to improve performance, it
26 further brings up the possibility of overfitting to the data. It can
27 further be argued that the performance of the 3D-printed com-
28 puter could also be improved by optimizing it according to the

task requirements. Nonetheless, the results emphasize the 1
importance of integrated memory in processing events. 2

2.2. Near-Sensor Data Processing 3

The 3D-printed computer was employed to process data from a 4
wearable device to detect the type of user activity as a demonstra- 5
tion of its real-life utility. In this case, the data from a 3-axis accel- 6
erometer on a wearable device worn on the wrist of a user during 7
different activities were collected. There is a strong correlation 8
between the acceleration data from the three different axes 9
(a_x, a_y, a_z). To simplify the problem, the acceleration data from 10
the three axes were combined to produce an equivalent signal 11

$$a_{eq} = \sqrt{a_x^2 + a_y^2 + a_z^2} \quad (1) \quad Q3$$

This signal was then used to extract features provided to the 12
3D-printed computer for activity detection. 13

The incoming data were studied in 5 s time frames. The mean, 14
standard deviation, root mean squared value, and the number of 15
peaks of a_{eq} in each time frame were calculated and normalized. 16
These features were then converted into analogue voltage signals 17
and applied to the 3D-printed computer as features of user 18
activity data in that time frame. The training was based on 19
196 instances of labeled user activity. The weights of the output 20
layer were determined through linear regression. The 21
performance of the computer was evaluated using 60 additional 22

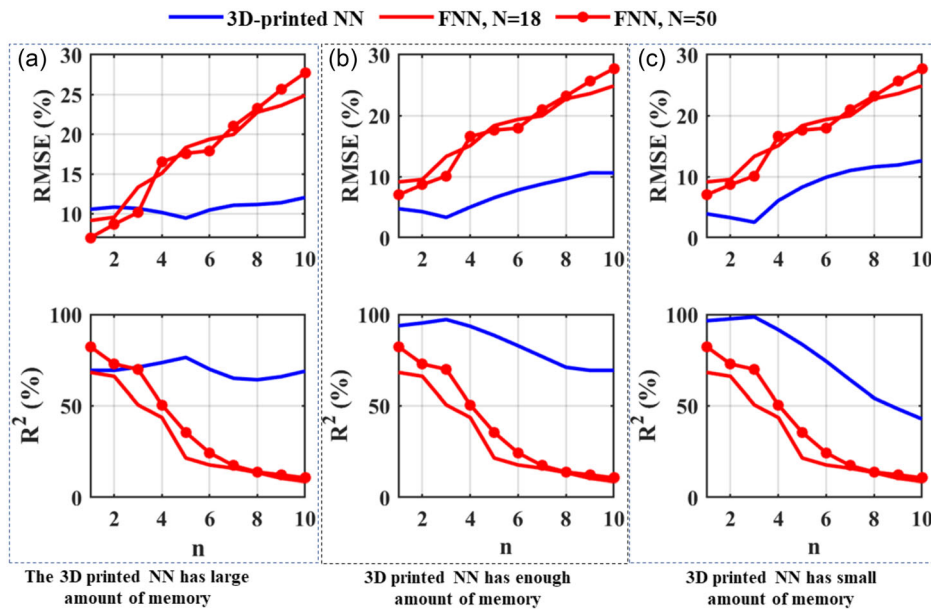


Figure 6. Comparison of the performance of the 3D-printed processor against feedforward neural networks. Two FNN were constructed and trained on the same data as the 3D printed sensor; their performances were compared by solving NARMA tasks with varying orders of nonlinearity and memory, represented by n on the horizontal axes: a) The 3D printed NN has large amount of memory; b) 3D printed NN has enough amount of memory; c) 3D printed NN has small amount of memory.

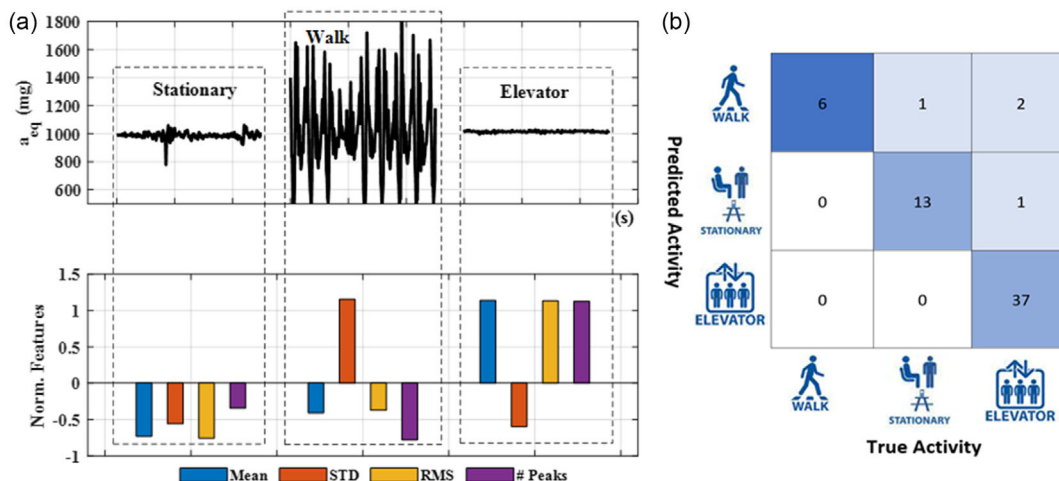


Figure 7. Performance of the computer in recognizing user activity from sensor data. a) Sample raw sensor data and normalized extracted features for different activities; b) performance of the 3D-printed computer in user activity detection based on acceleration data.

1 instances of labeled activities that were excluded from the
2 training dataset (i.e., validation set).

3 The results of this experiment are shown in **Figure 7**.
4 Figure 7a shows a sample of raw data collected from the accel-
5 erometers (a_{eq}) as well as features extracted from 5 s timeframes
6 for different activities. Figure 7b shows the performance of the
7 3D-printed computer in detecting patterns in the data after training.
8 As seen, the processor performs the data processing with
9 93.3% accuracy, and 92.5%, 92.8%, and 100% sensitivity in deter-
10 mining whether the user is in an elevator, stationary, or walking,
11 respectively. Note that the sampling period, in this case, is 5 s,

1 corresponding to a sampling frequency of about 12/TTC. This 1
2 level of performance for such a limited set of input features is 2
3 on par with the performance of typical machine learning 3
4 algorithms on the same data. 4

3. Conclusion

5 We demonstrated the first 3D-printed physical computer that 6
7 was built based on the concept of RC. In an RC, the responses 7
8 of nonlinear, coupled physical elements are used to create 8

1 context from incoming time-series data. The earlier work by
2 several research groups had demonstrated the possibility of
3 using reservoir computers based on photonic components,
4 memristors, and many other physical systems. However, most
5 of the reported physical RCs require sophisticated measurement
6 systems or highly specialized manufacturing processes that often
7 counteract the benefits offered by the approach. We demon-
8 strated the computational capabilities of our printed computer
9 using standard tasks and also used it to solve a real-life problem.

10 3D-printed computers based on our reported approach can be
11 designed and fabricated in any facility with access to regular 3D
12 printers that can print with both conductive and insulating fila-
13 ments. Even in the current first-attempt form, numerous ways
14 exist to increase the computer's computational capability without
15 significant practical barriers. Sample approaches include modu-
16 lating control signals, increasing the number of printed neurons,
17 increasing the number of layers, adjusting the lateral and vertical
18 distances between the neurons (and hence their coupling), and
19 varying trace widths. An optimal design of similar computers
20 should seek a balance between the aforementioned parameters.

21 Additionally, the presented work paves the way for the
22 realization of fully 3D-printed intelligent systems that combine
23 3D-printed sensors with a 3D-printed contextual computer
24 to instantly extract context from environmental changes.
25 Furthermore, the principles may be applied to other manufactur-
26 ing techniques, for instance, by using coupled temperature-
27 sensitive resistors on silicon chips to process data from
28 micromachined sensors and create context without digital
29 computations.

30 4. Experimental Section

31 **D Printing Setup:** FDM is the most widely used 3D printing technology.
32 It uses a filament spool fed to an extrusion head with a heated nozzle.
33 Once the extrusion head heats, it softens and lays down the heated mate-
34 rial at set locations, where it cools to create a material layer. The nozzle
35 then moves down to deposit the next layer. We used a double extrusion 3D
36 printer (Ultimaker 3) to print the reservoir.^[32] The material is printed with a
37 default nozzle size of 0.4 mm. The printer settings were adjusted to have a
38 layer height of 0.1 mm for each printed layer and a wall thickness of
39 0.8 mm. Thus, the minimum feature size for the conductive trace is
40 1.6 mm in the x and y directions, while it is 0.1 mm in the z-direction.

41 The key strength of FDM is the availability of a wide range of materials,
42 including thermoplastics such as PLA, a vegetable-based, biodegradable
43 thermoplastic. PLA is an electrical insulator, so it was used as the substrate
44 and insulating material between the conductive layers. Conductive traces
45 were printed using carbon-PLA composite filaments. We used 2.85 mm
46 pure PLA filament (Ultrafuse series from BASF) for the main structure
47 and 2.85 mm carbon-PLA composite (RM-PL0100 from Lulzbot) for
48 the conductive segments. Before 3D printing, the conductive PLA filament
49 has a volume resistivity of 15 Ω cm. A 3D-printed structure printed in the
50 x- or y- directions has a resistivity of 30 Ω cm, whereas 3D-printed layers
51 printed in the z-direction have a resistivity of 115 Ω cm. Multilayer resistors
52 offer higher conductivity as more conduction paths will be possible due to
53 the increased connections between carbon elements within this structure.
54 Silver conductive paste/epoxy was used to attach wires to the printed
55 contacts, which were cured on a hot plate at 50 °C for 1 h.

56 The lateral dimensions of the 3D-printed reservoir are 3.9 cm × 3.5 cm,
57 while its height depends on the thickness of the traces (i.e., the number of
58 printed layers). Conductive trace thicknesses vary from 0.5 to 2 mm, the
59 width of the conductive traces is 1.6 mm (the minimum feature size), and
60 the gap between the traces (layers) is 0.2 mm.

Data Collection Setup: For I-V characteristics, we swept the current
1 passing through the NTC forward and backward and measured its voltage
2 after various time intervals by Keysight 2901A precision source/measure
3 unit (SMU). The input signals and output data were collected using a
4 National Instruments PXIe-6363 I/O module through a LabVIEW interface
5 at a rate of one sample per second. The data for user activity detection
6 were collected using the SensorTile kit from STMicroelectronics, which
7 includes a pair of microcontrollers, a 3-axis accelerometer, and other
8 sensors.^[33] Training and test data were collected by attaching the module
9 to a user's wrist and recording data during different activities. 10

11 The input layer uses an analogue shift register to apply the signal and its
12 past three samples (i.e., $u(n)$, $u(n-1)$, $u(n-2)$, and $u(n-3)$) to the
13 reservoir. The readout layer runs a linear regression on the six signals
14 acquired from the reservoir in MATLAB.

15 **NARMA Task:** The nonlinear autoregressive moving average (NARMA)
16 is a discrete-time temporal task with an n^{th} -order time lag. The NARMA
17 time series is given by^[34]

$$y(t) = \alpha y(t-1) + \beta y(t-1) \sum_{i=1}^n y(t-i) + \gamma u(t-n)u(t-1) + \delta \quad (2)$$

18 where $\alpha = 0.3$, $\beta = 0.05$, $\gamma = 1.5$, and $\delta = 0.1$. The dependence of
19 NARMA on its nonlinearity and long time lags makes it a challenging
20 problem for any computational system. Calculating NARMA n task requires
21 a device capable of algorithmic programming and perfect memory of the
22 input and the outputs of up to n previous time steps.

23 **MC:** The short-term MC of the RC system is important in applications
24 requiring memory of past events. To evaluate the short-term MC, the
25 τ -delay MC (MC(τ)) is calculated from^[34]

$$\text{MC}(\tau) = \frac{\text{Cov}(u(t-\tau), y_{\tau}(t))}{\sigma^2(u(t)) \cdot \sigma^2(y_{\tau}(t))} \quad (3)$$

26 where $u(t-\tau)$ is a τ -step delayed input, $y_{\tau}(t) = u(t-\tau)$ is its reconstruction
27 at the output, $\text{Cov}(\cdot, \cdot)$ is the covariance of the two time-series signals, and
28 $\sigma^2(\cdot)$ is the variance of a signal. The overall short-term MC is then
29 approximated as

$$\text{MC} = \sum_{\tau=1}^{\infty} \text{MC}(\tau) \quad (4)$$

Supporting Information 30

Supporting Information is available from the Wiley Online Library or from
31 the author. 32

Conflict of Interest 33

The authors declare no conflict of interest. 34 Q5

Data Availability Statement 35

The data that support the findings of this study are available from the
36 corresponding author upon reasonable request. 37

Keywords 38

3D printing, additive manufacturing, reservoir computing, thermal
39 coupling 40

Received: February 15, 2023

Published online:

- 1
2
- Q6 3 [1] J. von Neumann, *First Draft of a Report on the EDVAC* **1945**.
4 [2] T. D. Ladd, F. Jelezko, R. Laflamme, Y. Nakamura, C. Monroe,
5 J. L. O'Brien, *Nature* **2010**, 464, 45.
6 [3] K. Roy, A. Jaiswal, P. Panda, *Nature* **2019**, 575, 607.
7 [4] F. Zhou, Y. Chai, *Nat. Electron.* **2020**, 3, 664.
8 [5] M. Lukoševičius, H. Jaeger, *Comput. Sci. Rev.* **2009**, 3, 127.
9 [6] G. Tanaka, T. Yamane, J. B. Héroux, R. Nakane, N. Kanazawa,
10 S. Takeda, H. Numata, D. Nakano, A. Hirose, *Neural Networks*
11 **2019**, 115, 100.
12 [7] J. C. Coulombe, M. C. A. York, J. Sylvestre, *PLoS One* **2017**, 12,
13 0178663.
14 [8] B. Barazani, G. Dion, J. F. Morissette, L. Beaudoin, J. Sylvestre,
15 *J. Microelectromech Syst.* **2020**, 29, 338.
16 [9] L. Appeltant, M. C. Soriano, G. Van Der Sande, J. Danckaert,
17 S. Massar, J. Dambre, B. Schrauwen, C. R. Mirasso, I. Fischer,
18 *Nat. Commun.* **2011**, 2.
19 [10] J. Moon, W. Ma, J. H. Shin, F. Cai, C. Du, S. H. Lee, W. D. Lu, *Nat.*
20 *Electron.* **2019**, 2, 480.
21 [11] M. J. Marinella, S. Agarwal, *Nat. Electron.* **2019**, 2, 437.
22 [12] Q. Xia, J. J. Yang, *Nat. Mater.* **2019**, 18, 309.
23 [13] F. Duport, A. Smerieri, A. Akrouf, M. Haelterman, S. Massar, *Sci. Rep.*
24 **2016**, 6.
25 [14] K. Vandoorne, P. Mechet, T. Van Vaerenbergh, M. Fiers, G. Morthier,
26 D. Verstraeten, B. Schrauwen, J. Dambre, P. Bienstman, *Nat.*
27 *Commun.* **2014**, 5.
28 [15] O. R. Lykkebø, S. Harding, G. Tufte, J. F. Miller, *Lect. Notes Comput.*
29 *Sci.* **2014**, 8553 LNCS, 267.
30 [16] M. Dale, S. Stepney, J. F. Miller, M. Trefzer, in *Proc. of the Int. Joint*
31 *Conf. on Neural Networks*, IEEE, Piscataway, NJ **2017**, pp. 2178–2185
- [17] H. O. Sillin, R. Aguilera, H.-H. Shieh, A. V. Avizienis, M. Aono, 1
A. Z. Stieg, J. K. Gimzewski, *Nanotechnology* **2013**, 24. 2
[18] A. J. Capel, R. P. Rimington, M. P. Lewis, S. D. R. Christie, *Nat. Rev.* 3
Chem. **2018**, 2, 422. 4
[19] M. R. Khosravani, T. Reinicke, *Sens. Actuators, A* 305, 111916 (**2020**). 5
[20] T. N. Mangoma, S. Yamamoto, G. G. Malliaras, R. Daly, *Adv. Mater.* 6
Technol. **2022**, 7, 1. 7
[21] Y. Tuchman, T. N. Mangoma, P. Gkoupidenis, Y. Van De Burgt, 8
R. A. John, N. Mathews, S. E. Shaheen, R. Daly, G. G. Malliaras, 9
A. Salleo, *MRS Bull.* **2020**, 45, 619. 10
[22] C. Bao, T. H. Kim, A. Hassanpoor Kalhori, W. S. Kim, *iScience* **2022**, 11
25, 104119. 12
[23] C. Wan, G. Chen, Y. Fu, M. Wang, N. Matsuhsa, S. Pan, L. Pan, 13
H. Yang, Q. Wan, L. Zhu, X. Chen, *Adv. Mater.* **2018**, 30, 1801291. 14
[24] X. Lin, Y. Rivenson, N. T. Yardimci, M. Veli, Y. Luo, M. Jarrahi, 15
A. Ozcan, *Science* **2018**, 361, 1004. 16
[25] H. Jaeger, *Scholarpedia* **2007**, 2, 2330. 17
[26] V. Shirmohammadli, B. Bahreyni in *2021 21st Int. Conf. on Solid-State* 18
Sensors, Actuators and Microsystems (Transducers), IEEE, Piscataway, 19
NJ, **2021**, pp. 1307–1310. 20
[27] V. Shirmohammadli, B. Bahreyni, *Adv. Mater. Technol.* **7**, 2200361. 21
[28] P. F. Flowers, C. Reyes, S. Ye, M. J. Kim, B. J. Wiley, *Addit. Manuf.* **2017**, 22
18, 156. 23
[29] W. Waheeb, R. Ghazali, H. Shah, in *2019 Int. Conf. on Computer and* 24
Information Sciences (ICIS) **2019**, pp. 1–5, [https://doi.org/10.1109/](https://doi.org/10.1109/ICISCI.2019.8716417) 25
[ICISCI.2019.8716417](https://doi.org/10.1109/ICISCI.2019.8716417). 26
[30] D. A. Jones, *Proc. R. Soc. London, Ser. A* **1978**, 360, 71. 27
[31] M. Inubushi, K. Yoshimura, *Sci. Rep.* **2017**, 7. 28
[32] Ultimaker 3, <https://ultimaker.com/3d-printers/ultimaker-3>. 29 Q8
[33] STEVAL-STLKT01V1 - SensorTile development kit - STMicroelectronics, 30
<https://www.st.com/en/evaluation-tools/steval-stlkt01v1.html>. 31
[34] F. Stelzer, A. Röhm, K. Lüdge, S. Yanchuk, *Neural Networks* **2020**, 124, 32
158. 33